Electron-impact excitation of Fe XXII: Comparative study of relativistic *R*-matrix and distorted-wave approaches

M. F. Gu
Department of Physics and Kavli Institute for Particle Astrophysics and Cosmology, Stanford University, Stanford, California 94305, USA
(Received 28 July 2004; published 6 December 2004)

An implementation of the Dirac *R*-matrix theory is presented and applied to the calculation of electron-impact excitation of B-like Fe XXII in the $n=2$ complex. A detailed comparison between the *R*-matrix and relativistic distorted-wave (DW) results is given. Contrary to the previous close-coupling studies of this ion, where significantly different background collision strengths are found for several transitions as compared with the DW results, we obtain excellent agreements between the two methods for most transitions, except for the weak transitions to the higher members of the $2p^3$ configuration, where significant channel-coupling effects are indeed present. We show that the discrepancies found in the previous Dirac *R*-matrix calculation for dipole transtions at high energies are due to the nonconvergence of partial wave summation, despite the explicit inclusion of partial waves up to $l=40$. The reason for large differences in the threshold energy region for some transitions between the present and previous Dirac *R*-matrix results is not clear. We also show that the independent-process, isolated-resonance approximation within the DW framework can describe the near-threshold resonances reasonably well for this ion.

DOI: 10.1103/PhysRevA.70.062704 PACS number(s): 34.80.Kw

I. INTRODUCTION

The electron-impact excitation of B-like Fe XXII has been studied extensively in the past. Reference [1] calculated all $\Delta n=0$ collision strengths within the $n=2$ complex using a relativistic distorted-wave (RDW) approximation. The nonrelativistic *R*-matrix method coupled with a term-coupling-coefficient (TCC) transformation was applied to the B-like isoelectronic sequence including Fe XXII [2]. References [3,4] used a relativistic *R*-matrix code employing the Breit-Pauli (BP) Hamiltonian to calculate the collision strengths of Fe XXII within the $n=2$ and 3 complexes. A fully relativistic Dirac *R*-matrix atomic code (DARC) was also used to study the collisional excitation within the $n=2$ complex [5]. These previous studies have established the importance of both relativistic effects and the near-threshold resonances for this ion.

However, there is widespread confusion on the reliability of RDW results even when only the background collision strengths are concerned. The collision strengths in the nonresonant energy region do not always agree with the RDW results even for some strong dipole-allowed transitions. For example, both TCC and DARC calculations show that the background collision strength of $2s^22p(^2P_{1/2})-2s2p^2(^2D_{3/2})$ is about a factor of 2 smaller than the RDW results at energies below the highest thresholds of $n=2$ states. The DARC calculation also indicates that the collision strengths of dipole transitions at high energies are significantly smaller than the RDW results, even though the convergence of the partial-wave summation has been reportedly verified. The close-coupling collision strengths of the intercombination transition $2s^22p(^2P_{1/2})-2s2p^2(^4P_{1/2})$ were also shown to be quite different from the RDW calculation at the resonance-free energy region. Because the RDW method is inherently simpler and less ambitious, it is often assumed that such differences are due to the channel-coupling effects not included in the RDW approximation.

Another widely debated issue is whether the independent-process isolated-resonance approximation implemented within the DW framework can reasonably describe the near-threshold resonances for highly charged ions such as Fe XXII. No firm conclusions have resulted from the comparisons of close-coupling and DW results, because either the resonances included in DW calculations are not complete, or the target descriptions are not equivalent.

In an effort to address these issues, we have developed an implementation of the Dirac *R*-matrix theory that shares the same code for atomic structure with an existing RDW program. Both the *R*-matrix code and the RDW code are now parts of the integrated atomic software package, the Flexible Atomic Code [6]. In the present work, we apply both methods to the calculation of collision strengths for B-like Fe XXII within the $n=2$ complex. The atomic structure descriptions of the targets in the two methods are deliberately kept identical, which is the result of a relativistic configuration-interaction calculation including only the $1s^22l^3$ configurations. We demonstrate in this paper that the Dirac *R*-matrix collision strengths in the resonance-free energy region agree with the RDW results to within a few percent for most transitions, including those for which large discrepancies between close-coupling and RDW calculations have been found in the previous studies. Our RDW collision strengths also agree very well with the previous RDW calculation. Therefore, we argue that the differences between the previous close-coupling and RDW results are due to the problems in the particular *R*-matrix calculations. In fact, we show that the discrepancies for dipole-allowed transitions at high energies found by Ref. [5] are due to the nonconvergence of partial wave summation in their calculation, despite the inclusion of partial waves up to $l=40$. We also show that the

Coulomb-Bethe approximation for large partial waves is very accurate and can be safely used as a top-up procedure to obtain reliable total collision strengths for allowed transitions. The reason for the discrepancies in the low energy region is less clear, and difficult to identify without a detailed examination and comparison of different *R*-matrix implementations.

We also examine the accuracy of the isolated-resonance approximation for the treatment of near-threshold resonances, and find that for excitations of the $n=2$ states in Fe XXII, this method gives satisfactory results for most transitions. Although the fine details of the individual resonances are not identical in the isolated-resonance DW and Dirac *R*-matrix calculations, the resulting thermal effective collision strengths or rate coefficients differ by less than $\sim 10-20\%$. The present Dirac *R*-matrix implementation does not include radiation damping effects. However, it is relatively easy to include that in the isolated-resonance DW calculations, and we find radiation damping effects to be minimal for this ion ($<10\%$); they appear to be far less important than those found by Ref. [4] for the same transitions, where reductions of 10–20% were reported.

We find the channel-coupling effects to be indeed important for weak excitations to the higher members of the $n=2$ states, which belong to the $2p^3$ configuration. In fact, for these transitions, the configuration interaction between the $n=2$ and 3 complexes in the target is equally important, and it is expected that the channel coupling to the $n=3$ states is also non-negligible [4]. Therefore, for an accurate treatment of excitations to these levels, the target expansion must include $n=3$ configurations.

II. THEORETICAL METHOD

A. *R*-matrix internal region

The theoretical basis of the Dirac *R*-matrix method was described in Ref. [7], and a numerical implementation, DARC, was developed in Ref. [8]. The present work is a reimplementation of the same theory. As in the nonrelativistic case [9], the configuration space is partitioned into two regions separated by the *R*-matrix boundary r_0. r_0 is chosen such that the exchange between the incident electron and the target electrons is negligible for $r>r_0$. In the inner region, the total scattering wave function is expanded on a basis set

$$\Psi_k = \sum_{ij} c_{ijk} \mathcal{A}[\Phi_i, \phi_{ij}] + \sum_m d_{mk} \theta_m, \tag{1}$$

where Φ_i is the wave function of the target states, ϕ_{ij} is the *R*-matrix basis for the continuum electron, θ_m are the $(N+1)$-electron correlation wave functions introduced to compensate for the orthogonality constraints imposed on ϕ_{ij}, and $\mathcal{A}$ represents the angular coupling and asymmetrization between the target and incident electrons. The coefficients c_{ijk} and d_{mk} are derived by diagonalizing the $(N+1)$-electron Hamiltonian matrix, which is the standard Dirac-Coulomb Hamiltonian.

The *R*-matrix radial basis functions satisfy the boundary condition

$$\frac{\mathcal{Q}_i(r_0)}{\mathcal{P}_i(r_0)} = \frac{b+\kappa}{2r_0 c}, \tag{2}$$

where $\mathcal{P}_i$ and $\mathcal{Q}_i$ are the large and small components of the Dirac spinor for the basis wave function, c is the speed of light, κ is the relativistic angular momentum quantum number, and b is an arbitrary constant usually chosen to be 0. The multichannel scattering wave functions then satisfy the following boundary condition:

$$P_i(r_0) = \sum_j R_{ij}[2r_0 c Q_j(r_0) - (b+\kappa_j) P_j(r_0)], \tag{3}$$

where R_{ij} is the *R* matrix defined by

$$R_{ij} = \frac{1}{2r_0} \sum_k \frac{w_{ik}(r_0) w_{jk}(r_0)}{E_k^{N+1} - E}, \tag{4}$$

where w_{ik} are the surface amplitudes of Ψ_k in channel i, E_k^{N+1} are the *R*-matrix poles, and E is the total energy of the scattering system.

The summation in the *R*-matrix definition is truncated in practice, and the contributions from the distant poles are accounted for by the Buttle correction [10].

B. *R*-matrix external region

In the external region, the exchange between the scattered electron and the target electrons is neglected, the channel wave functions satisfy the coupled differential equations

$$\frac{dP_i}{dr} + \frac{\kappa_i}{r} P_i - \left(2c + \frac{\varepsilon_i}{c} + \frac{z}{cr}\right) Q_i = -\frac{1}{c} \sum_j \sum_{\lambda \geq 1} \frac{a_{ij}^{\lambda}}{r^{\lambda+1}} Q_j,$$

$$\frac{dQ_i}{dr} - \frac{\kappa_i}{r} Q_i + \left(\frac{\varepsilon_i}{c} + \frac{z}{cr}\right) P_i = \frac{1}{c} \sum_j \sum_{\lambda \geq 1} \frac{a_{ij}^{\lambda}}{r^{\lambda+1}} P_j, \tag{5}$$

where ε_i is the channel energy, z is the residual charge $Z-N$, and the asymptotic multipole coefficients a_{ij}^{λ} are defined as

$$a_{ij}^{\lambda} = \left\langle \Phi_i, \phi_i \left| \sum_k r_k^{\lambda} P_{\lambda}(\hat{r}_k \cdot \hat{r}_{N+1}) \right| \Phi_j, \phi_j \right\rangle, \tag{6}$$

where P_{λ} is the Legendre polynomial, and the integration in the angular and radial spaces is carried out except for the radial coordinate of the continuum electron.

The reactance K matrix is defined through the standard asymptotic form of the channel wave functions as described in Ref. [11]. The matching of the external and internal solutions at r_0 gives the K matrix. The S matrix and T matrix are given in terms of the K matrix as

$$S = \frac{1+iK}{1-iK},$$

$$T = S - 1, \tag{7}$$

where these matricies have particular total angular momentum and parity values J and π, respectively. The partial collision strength for a transition from target state a to b is a

TABLE I. The target states of B-like Fe XXII within the $n=2$ complex.

Level	J^π	Configuration	*LS* coupled	Energy (eV)	NIST (eV)
1	$1/2^-$	$2s^2_{1/2}2p_{1/2}$	$^2P_{1/2}$	0.0	0.0
2	$3/2^-$	$2s^2_{1/2}2p_{3/2}$	$^2P_{3/2}$	14.62	14.66
3	$1/2^+$	$2s_{1/2}2p^2_{1/2}$	$^4P_{1/2}$	49.68	50.16
4	$3/2^+$	$2s_{1/2}2p_{1/2}2p_{3/2}$	$^4P_{3/2}$	56.49	57.06
5	$5/2^+$	$2s_{1/2}2p_{1/2}2p_{3/2}$	$^4P_{5/2}$	63.11	63.64
6	$3/2^+$	$2s_{1/2}2p_{1/2}2p_{3/2}$	$^2D_{3/2}$	92.29	91.32
7	$5/2^+$	$2s_{1/2}2p^2_{3/2}$	$^2D_{5/2}$	94.97	94.18
8	$1/2^+$	$2s_{1/2}2p_{1/2}2p_{3/2}$	$^2P_{1/2}$	107.30	105.82
9	$1/2^+$	$2s_{1/2}2p^2_{3/2}$	$^2S_{1/2}$	122.54	121.28
10	$3/2^+$	$2s_{1/2}2p^2_{3/2}$	$^2P_{3/2}$	124.79	123.03
11	$3/2^-$	$2p^2_{1/2}2p_{3/2}$	$^4P_{3/2}$	156.14	155.69
12	$3/2^-$	$2p_{1/2}2p^2_{3/2}$	$^2D_{3/2}$	174.95	173.13
13	$5/2^-$	$2p_{1/2}2p^2_{3/2}$	$^2D_{5/2}$	178.68	176.91
14	$1/2^-$	$2p_{1/2}2p^2_{3/2}$	$^2P_{1/2}$	196.87	194.61
15	$3/2^-$	$2p^3_{3/2}$	$^2P_{3/2}$	203.85	201.81

summation over the channels $\alpha_a J_a \kappa_a$ to $\alpha_b J_b \kappa_b$ that are coupled to give total J and π, where α represents all other quantum numbers required to uniquely identify a target state. The total collision strength is given by

$$\Omega_{ab} = \frac{1}{2}\sum_{J\pi}(2J+1)\sum_{\kappa_a\kappa_b}|T^{\kappa_a\kappa_b}_{ab}|^2. \tag{8}$$

However, the direct integration of Eq. (5) from the radius where the asymptotic form applies to r_0 is not only inefficient but also unstable when some channels are closed. In the present implementation, we use the relativistic extension of the *R*-matrix propagation method [12]. Several additional zones are used to propagate the *R* matrix at r_0 to a large radius, where the solution is matched to the uncoupled Dirac-Coulomb wave functions to obtain the *K* matrix. In the present calculation, r_0 is chosen to be 1.4, and the final matching radius is 10.0 in atomic units. As we verify later, our results have converged with respect to the matching radius.

C. Target states

A relativistic configuration-interaction program as implemented in the Flexible Atomic Code [6] is used to derive target wave functions and energies. The configuration basis includes $2s^22p$, $2s2p^2$, and $2p^3$ configurations. The *R*-matrix target expansion includes the same set of configurations. In Table I, we list the configuration designation and energies of the 15 states in the $n=2$ complex. The target energies agree with the experimental values from the atomic spectroscopic database at the National Institute of Standard and Technology to within a fraction of eV for low lying members and 1–2 eV for higher ones.

D. Scattering calculations

Partial waves up to $l=40$ and 25 radial basis functions per partial wave are included in the *R*-matrix calculation. To map out the fine details of the resonance structure, a mesh of 5×10^{-3} eV is used at energies below 205 eV, which is slightly larger than the highest threshold in the $n=2$ complex. We find that with a mesh of 5×10^{-3} Ry used in Ref. [5], the resonances are not sufficiently well resolved. At high energies up to 2.5 keV, the collision strengths are calculated with a coarse mesh of 75 eV steps.

A relativistic DW method is also used to calculate the same set of collision strengths, with the identical target description. The computational method for the background DW collision strengths is similar to that of Ref. [13]. The near-threshold resonances are also calculated in the independent-process, isolated-resonance approximation, in which the excitation from state *a* to *b* is treated as a two-step process, dielectronic capture forming a doubly excited state *d* which is followed by autoionization into state *b*. The resonance contribution to the collision strength is expressed as

$$\Omega_{ab} = \sum_d \pi g_d A^a_{da}\frac{A^a_{db}}{\sum_i A^a_{di}+\sum_k A^r_{dk}}\delta(E-E_{ad}), \tag{9}$$

where g_d is the statistical weight of the doubly excited state *d*, A^a is the autoionization rate, A^r is the radiative decay rate, and E_{ad} is the resonance energy. The resonance profile is approximated with a δ function. The summation over the doubly excited states includes all $2l^3nl'$ configurations with $n\leqslant 80$.

A separate RDW calculation is carried out with the inclusion of configuration interaction between the $n=2$ and 3 complexes. The results are used to check their effects on the collision strengths.

III. RESULTS

In this section, we compare the present *R*-matrix and RDW results with previous close-coupling and RDW calculations for some representative transtions from the ground state.

A. Resonance energy region

First, we examine the weak transition 1-2, i.e., from level 1 to level 2. Because the collision strength in this energy region is dominated by numerous narrow and dense resonances, we convolve the calculated collision strengths with a Gaussian function of full width at half maximum (FWHM) 2.35 eV (i.e., a standard deviation of 1 eV) in the graphical representation. With such an energy resolution, the true effects of resonances are easier to see while individual peaks corresponding to Rydberg series can still be distinguished. In Fig. 1, we show the present *R*-matrix and RDW results. The RDW results include those without resonances and those with resonances treated in the isolated-resonance approximation. The background collision strength in the previous close-coupling calculations agrees very well with the DW result. The present results for the background values are also in very

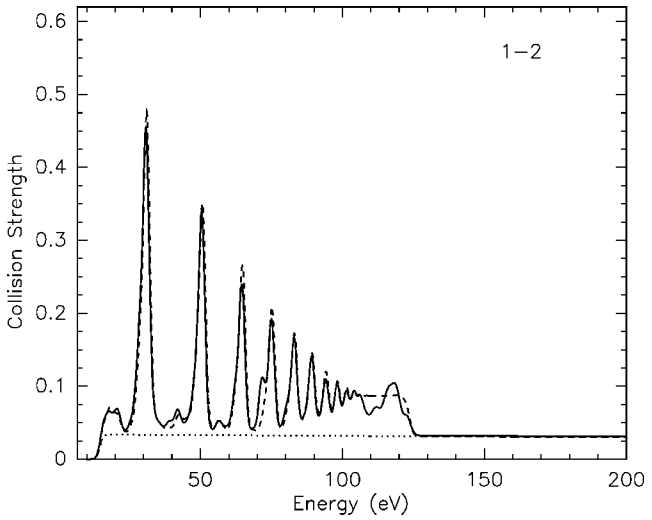

FIG. 1. The collision strength of the transition 1-2 in the resonance energy region. The resonances have been convolved with a Gaussian function of FWHM 2.35 eV. The solid line is the present *R*-matrix result, the dotted line is the present RDW background, and the dashed line is the isolated-resonance DW result.

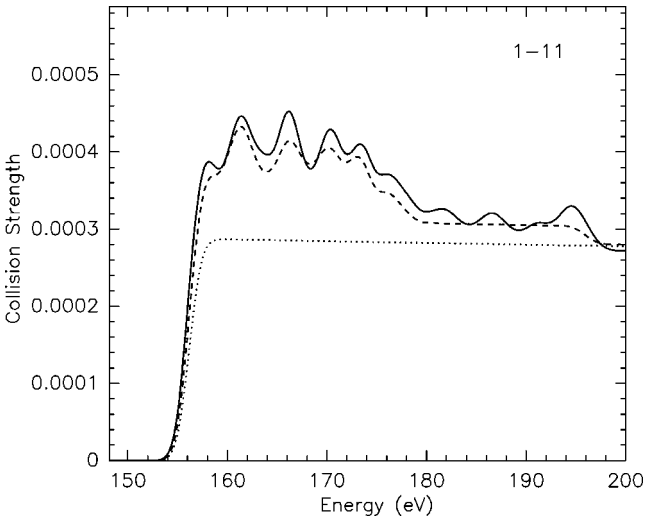

FIG. 2. Same as Fig. 1, but for the transition 1-11.

good agreement with each other, and with the previous calculations. This transition is most affected by the resonances, because the upper level is within the ground configuration and has low excitation threshold. Figure 1 clearly shows the resonance peaks converging to the $2s2p^2$ thresholds. The isolated-resonance DW collision strengths shown are calculated without radiation damping effects, as are the present *R*-matrix results. The radiation damping effects are discussed later in the paper. The isolated-resonance approximation is found to give almost identical resonance structure in both position and strength for this transition. As we discuss later, the resonance contributions to the thermal rate coefficients for this transition are significantly smaller in the present calculation than in the BP *R*-matrix results [4]. The DARC calculation [5] did not give thermaly averaged effective collision strengths or rate coefficients, and we are not able to make a detailed comparison.

The background collision strength of transition 1-11 is predicted to be 2.7×10^{-4} in the DARC, 1.85×10^{-4} in the TCC, and 3.0×10^{-4} in the previous RDW calculations. In the present calculation, both the *R*-matrix and RDW methods give a value of 2.8×10^{-4} as shown in Fig. 2. This is very close to the DARC and previous RDW results, but differs from the TCC result. The isolated-resonance approximation is also found to give excellent results for the resonance contributions.

Excitations from the ground state to levels 3 and 5 are intercombination transitions. The previous DARC and TCC background collision strengths for 1-3 are different from the RDW results by 40-50%, while those for 1-5 agree with the RDW results. In the present *R*-matrix calculation, the background collision strengths for both transitions agree with the present and previous RDW results, which have the values of 0.011 and 0.005, respectively. As shown in Figs. 3 and 4, the disagreement between isolated-resonance DW and the *R*-matrix collision strengths is slightly worse than for the previous two transitions. The discrepancies are mostly seen for the resonance groups between 80 and 100 eV. Nevertheless, the overall contributions of resonances to the collision strengths are seen to be similar in the two methods.

One of the most puzzling facts in the previous close-coupling results is that the background collision strength of the strong dipole-allowed transition 1-6 is a factor of 2 smaller in the DARC and TCC than in the RDW calculations at energies below the highest threshold of the $n=2$ complex. In Fig. 5, we show that the present *R*-matrix and RDW collision strengths are practically identical with values of 0.25-0.26 below 200 eV, which also agrees very well with the previous RDW calculation. The effects of resonances are minimal for this transition, and after convolution with the Gaussian function, only a small bump is seen around 100 eV.

The RDW values of other dipole transitions from the ground state, namely, 1-8, 1-9, and 1-10 are also found to be larger than the DARC results. In the present calculation, we find that the *R*-matrix and RDW results all agree to within a

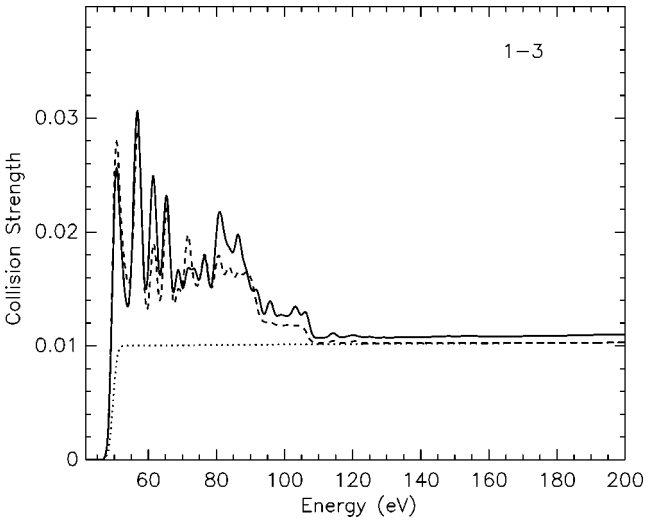

FIG. 3. Same as Fig. 1, but for the transition 1-3.

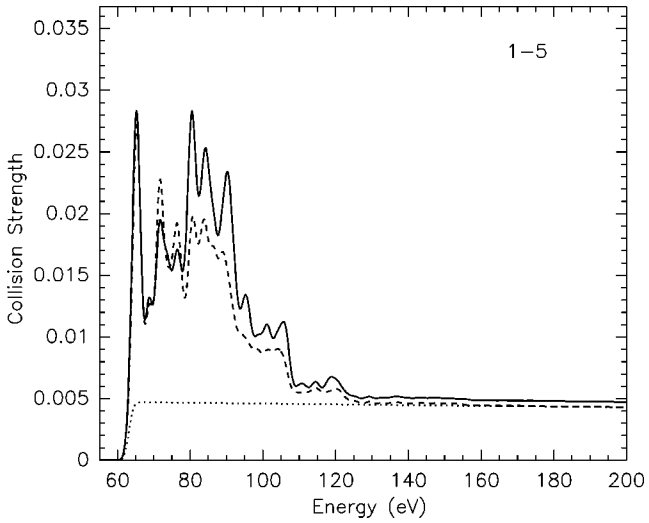

FIG. 4. Same as Fig. 1, but for the transition 1-5.

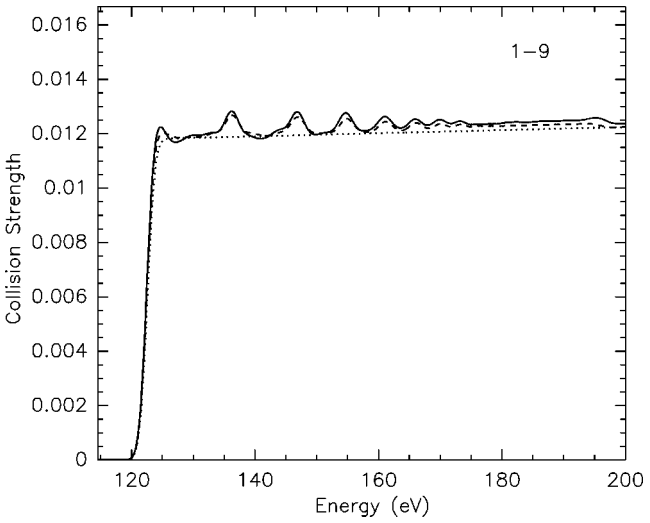

FIG. 6. Same as Fig. 1, but for the transition 1-9.

few percent, and also agree with the previous RDW calculation. An example is shown in Fig. 6 for the transition 1-9. This transition is relatively weak, with a background collision strength of 0.012 at 200 eV. Resonances, although weak, are noticeable at low energies. We also find the isolated-resonance approximation to agree with the *R*-matrix results very well.

The previous DARC calculation also exhibits a strange behavior, i.e., the agreements between the DARC and RDW results for these dipole transitions are usally good at energies immediately above the highest threshold of the $n=2$ complex. For example, the collision strength of the transition 1-6 at 20 Ry is shown to be 0.27, which agrees with RDW and the present results. At energies near 10 Ry, the collision strength becomes 0.12. Therefore, there is an abrupt jump in the background collision strength across the threshold region. Such a jump is unlikely to be physical, and we suspect that there might have been numerical problems in the DARC calculation at low energies.

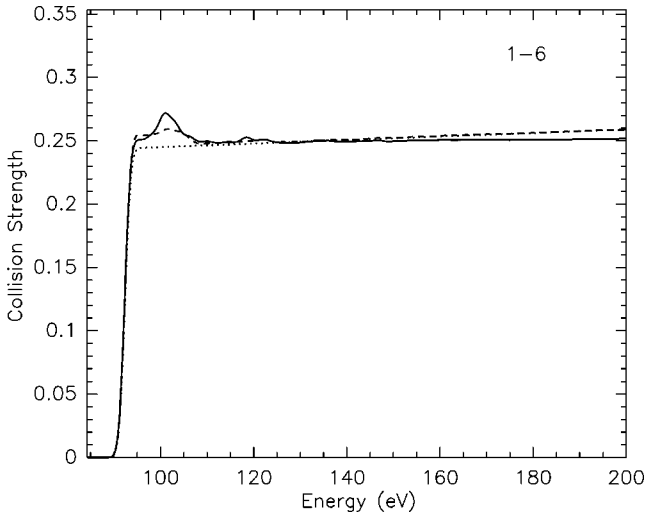

FIG. 5. Same as Fig. 1, but for the transition 1-6.

B. High energy region

Another puzzling fact in the previous DARC calculation is that the collision strengths of dipole transitions are consistently smaller than the RDW results at energies above ~100 Ry. The RDW collision strengths continue to rise as energy goes higher, while the DARC results start to level off and eventually decrease above 150 Ry. Such behavior is a classic symptom of nonconvergence in the partial-wave summation. At these high energies, the high partial-wave contributions become significant, and are usually included in the RDW calculations with the Coulomb-Bethe approximation (CBA). However, in the DARC calculation, the authors claim that their results are 100% converged for the weak transitions, and nearly converged for the stronger ones, and suggest that the CBA contributions in the RDW results may have been overestimated. Here we show that the convergence could not have been reached for the dipole transitions with partial-waves $l \leqslant 40$ at energies above 150 Ry.

In Fig. 7, we show the collision strength of the transition 1-6 at energies from 200 to 2500 eV. It is seen that the *R*-matrix result agrees with the RDW at energies below 1200 eV, and starts to fall below the RDW collision strength at higher energies, as is found in the previous DARC calculation. In Fig. 8, we show the partial-wave contributions to the total collision strength of this transition at an energy of 2.45 keV. The solid line represents the *R*-matrix results, the filled circles are the present RDW calculation, and the dashed line is obtained with the CBA. Note that in the present RDW calculation the partial collision strengths are calculated for a few partial waves when $8 \leqslant l \leqslant 36$, and interpolation is used to carry out the summation, which is a highly accurate procedure. In addition, we only calculate the ratios of CBA collision strengths in successive partial waves with the recursive relation [14], and the curve shown in Fig. 8 is normalized to the RDW collision strength at $l=36$. It is clear that the RDW partial collision strengths agree with the *R*-matrix results almost perfectly for all *l*, while CBA results become highly accurate for $l \geqslant 10$. If we estimate the $l>40$ contributions with the CBA collision strengths, we obtain a

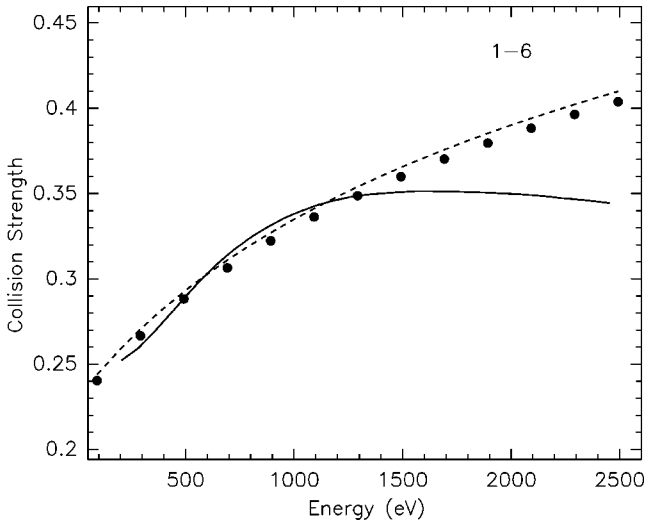

FIG. 7. The collision strength of the transition 1-6 in the high energy region. The solid line is the present *R*-matrix result. The dashed line is the present RDW result. The filled circles are the RDW results with additional configuration interaction between the $n=2$ and 3 complexes in the target.

value of 0.07. The present *R*-matrix total collision strength at this energy is 0.344, and the RDW with CBA top-up gives a value of 0.409. Once the CBA contribution for $l>40$ is added to the *R*-matrix result, it agrees with the RDW collision strength to within 2%. Therefore, the partial-wave summation with $l\leqslant 40$ has only converged to about 85% of the total collision strength at 2.45 keV for the transition 1-6, and a CBA top-up procedure accurately accounts for the missing contributions. We find similar results for all other dipole transitions, and when CBA is used to complete the summation, the *R*-matrix collision strengths agree with the RDW results to within a few percent.

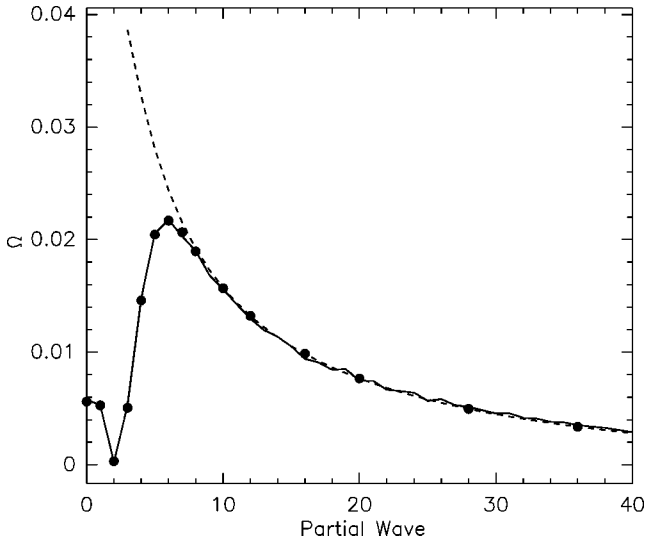

FIG. 8. The partial collision strengths with $l\leqslant 40$ for the transition 1-6 at an energy of 2.45 keV. The solid line is the present *R*-matrix result. The filled circles are the present RDW calculations. The dashed line is the Coulomb-Bethe approximation.

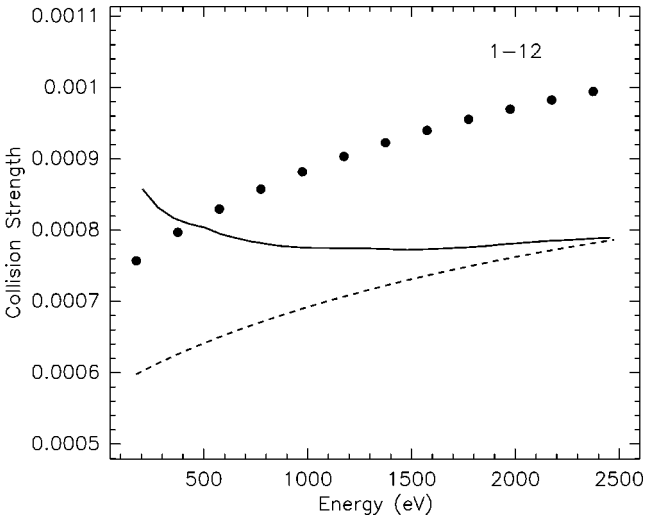

FIG. 9. Same as Fig. 7, but for the transition 1-12.

The agreements between the present *R*-matrix and RDW results for other types of transitions are generaly good to within a few percent in the entire high energy region, except for some transitions whose upper levels belong to the $2p^3$ configuration. As examples, we show the results for transitions 1-12 and 1-14 in Figs. 9 and 10. For the transition 1-12, there is good agreement at high energies above 2 keV, but the RDW collision strengths is appreciably smaller than the *R*-matrix results at energies below 1 keV. For the transition 1-14, the discrepancy is large throughout the entire energy region between 200 and 2500 eV. Note that the excitations from the ground state to these levels are very weak, because they are connected by two-electron transitions. It appears that for these transitions the channel-coupling effects are indeed important.

However, these transitions are also heavily affected by the configuration interaction between the $n=2$ and 3 target configurations. As shown in Figs. 9 and 10 by filled circles, when such configuration interaction is included in the RDW calculation, the collision strengths may change by significant

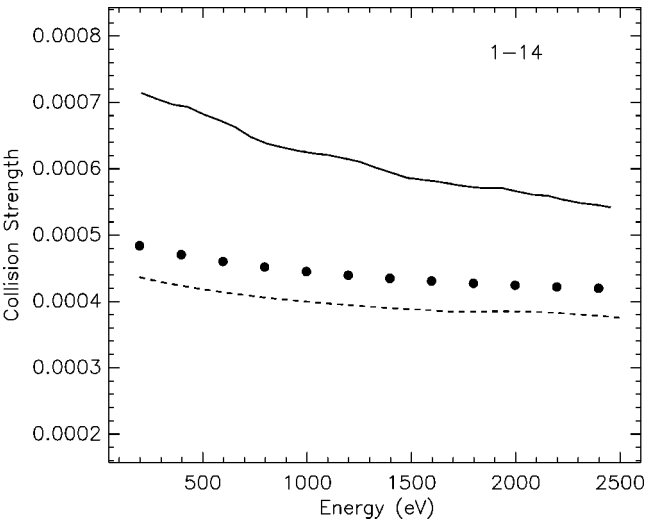

FIG. 10. Same as Fig. 7, but for the transition 1-14.

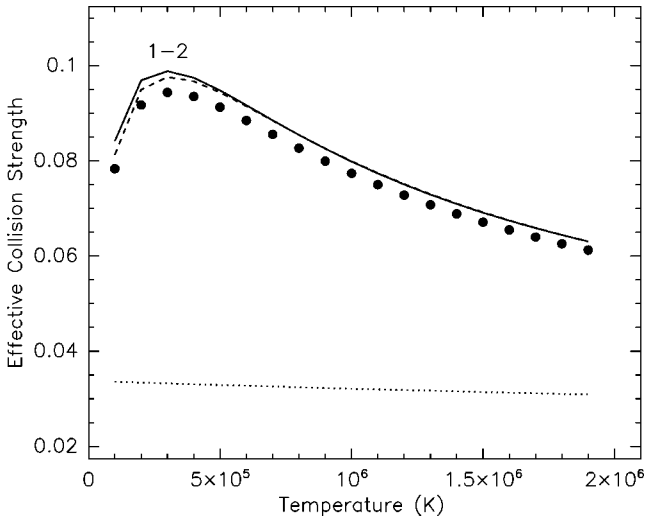

FIG. 11. The effective collision strength of the transition 1-2. The solid line is the present *R*-matrix result. The dotted line is the present RDW result. The dashed line is the isolated-resonance DW calculation without radiation damping. The filled circles are the isolated-resonance DW results with radiation damping.

amounts. In contrast, the configuration-interaction effect is minimal for the transition 1-6, and all other transitions discussed above. As shown in Ref. [4], the transitions to $2p^3$ states are also most affected by channel coupling to the $n=3$ complex. Therefore, it appears that an *R*-matrix calculation with target expansion including $n=3$ states must be used in these cases.

C. Effective collision strengths and radiation damping

In Figs. 11–14, we show some examples of the thermally averaged effective collision strengths for temperatures between 0.1×10^6 and 2×10^6 K. It is seen that the resonances enhance the effective collision strength by as much as a factor of a few over the RDW background values. The isolated-resonance approximation DW results give reasonably accurate effective collision strengths, which agree with the *R*-matrix results to within 10–20 %.

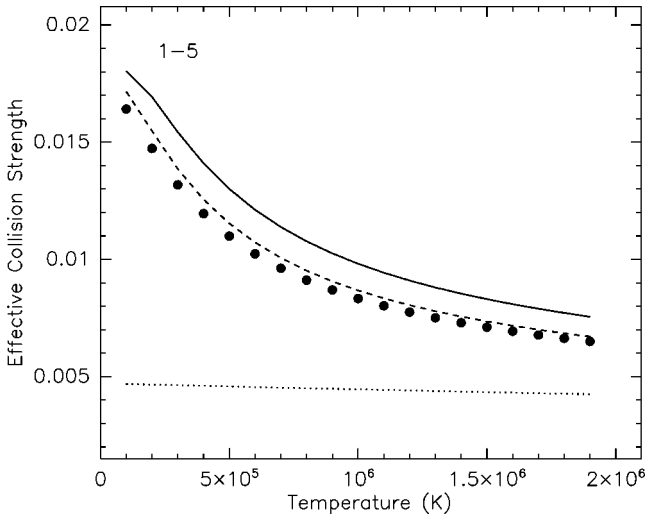

FIG. 13. Same as Fig. 11, but for the transition 1-5.

It has been reported that radiation damping of the resonances is important for some transitions [4]. In particular, it has been found that the radiation damping reduces the effective collision strengths of the transition 1-2 by ~15%. The present *R*-matrix calculation does not include radiation damping effects. However, we inlude the radiation damping in a separate isolated-resonance DW calculation to study its effect. The resulting effective collision strengths are shown in Figs. 11–14 with filled circles. We find the reduction over the corresponding values without damping to be within 10%, and it is far less important than that reported in Ref. [4].

The effective collision strengths in the present work are significantly different from those of Ref. [4] for some transitions. For example, at a temperature of 4.4×10^5 K, the present effective collision strength for the transition 1-2 is ~50% smaller than the damped result of Ref. [4]. For the transition 1-3, the present *R*-matrix result is about 40% larger. For the transitions 1-6 and 1-9, the present results are

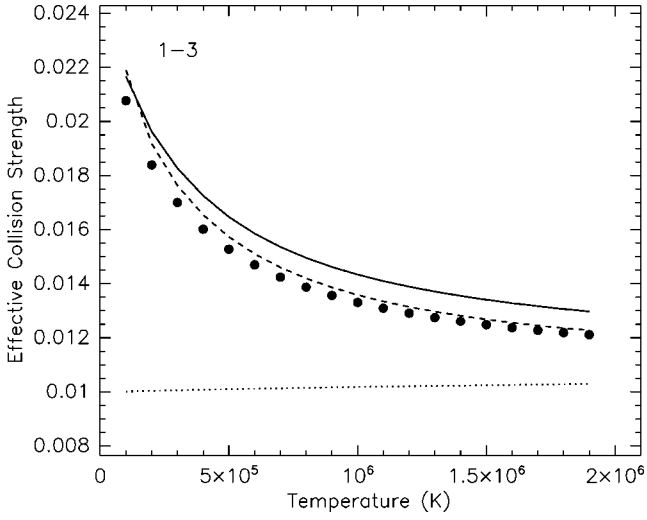

FIG. 12. Same as Fig. 11, but for the transition 1-3.

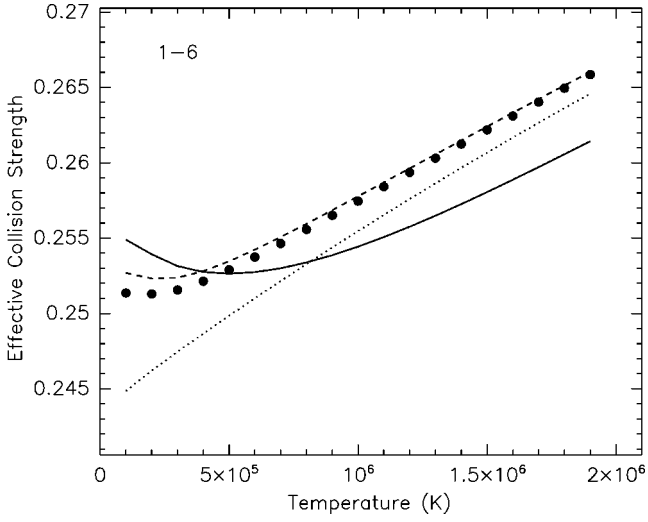

FIG. 14. Same as Fig. 11, but for the transition 1-6.

TABLE II. Comparison of the present *R*-matrix and isolated-resonance DW effective collision strengths with the 15-term BP *R*-matrix results including radiation damping [4] for transitions from the ground state at a temperature of 4.41×10^5 K. The notation $a[b]$ means $a\times10^b$.

Level	Present *R* matrix	DW (no damping)	DW (damping)	BP *R* matrix
2	9.63[−2]	9.57[−2]	9.26[−2]	1.51[−1]
3	1.69[−2]	1.62[−2]	1.57[−2]	1.21[−2]
4	1.55[−2]	1.36[−2]	1.31[−2]	1.31[−2]
5	1.36[−2]	1.21[−2]	1.16[−2]	1.29[−2]
6	2.53[−1]	2.53[−1]	2.52[−1]	1.79[−1]
7	9.15[−3]	8.11[−3]	7.52[−3]	1.09[−2]
8	2.69[−1]	2.70[−1]	2.70[−1]	2.27[−1]
9	1.23[−2]	1.22[−2]	1.22[−2]	8.69[−3]
10	5.40[−2]	5.46[−2]	5.46[−2]	4.47[−2]
11	3.38[−4]	3.30[−4]	3.28[−4]	4.74[−4]
12	8.88[−4]	6.21[−4]	6.20[−4]	9.88[−4]
13	5.27[−4]	4.12[−4]	4.10[−4]	5.33[−4]
14	7.11[−4]	4.33[−4]	4.33[−4]	4.51[−4]
15	1.01[−4]	6.12[−5]	6.12[−5]	9.23[−5]

also 40% larger, which indicates that the BP *R*-matrix collision strengths for these dipole transitions are also much smaller than the RDW results. A comparison of the effective collision strengths between the present *R*-matrix isolated-resonance DW and the previous 15-term BP *R*-matrix results is shown in Table II for transitions from the ground state.

D. Effects of the *R*-matrix matching radius

In the present *R*-matrix calculation, the *R* matrix at r_0 is propagated over two zones to a radius of $r_1=10.0$ a.u., where the matching to the uncoupled Dirac-Coulomb wave functions gives the *K* matrix. We have verified that our results have converged with respect to the matching radius. To do so, we directly integrate Eq. (5) from a larger radius $r_2=30.0$ a.u. to r_1 and r_0, using the Dirac-Coulomb wave functions as the initial condition, and including the $\lambda=1$ and 2 terms in the multipole potential. The matching is then carried out at either r_1 using the propagated *R* matrix, or at r_0 using the original *R* matrix. Because the direct integration is stable only when all channels are open using our simple implementation of the integration method, we carry out such calculations only for energies above the highest threshold. We obtain identical results for all transitions independent of whether the matching is performed at r_1 or r_0, indicating that our *R*-matrix propagation method is correct. For all forbidden and intercombination transitions, we also obtain the same results as when no integration is done and matching is performed at r_1 with Dirac-Coulomb wave functions. For dipole-allowed transitions, only small differences on the order of a few percent are seen. As an example, we show the comparison for the transition 1-6 in Fig. 15. Therefore, we

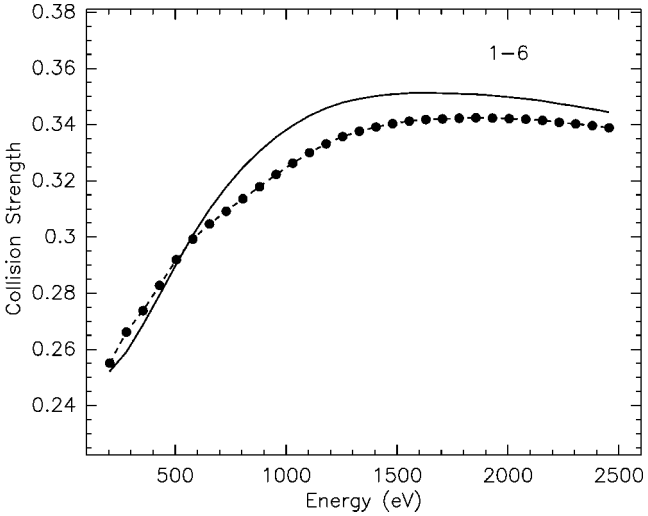

FIG. 15. The effects of *R*-matrix matching radius on the transition 1-6. The solid line is the present *R*-matrix result with a matching radius of 10.0 using Dirac-Coulomb wavefunctions. The dotted line is for a matching radius of 10.0 using the solution integrated inward from $r=30.0$. The filled circles are for a matching radius of 1.4 using the solution integrated inward from $r=30.0$.

conclude that at the matching radius of 10.0, the uncoupled Dirac-Coulomb wave functions are good approximations for the scattering system.

IV. CONCLUSIONS

In conclusion, we have presented an implementation of the relativistic *R*-matrix theory, and its application to the electron-impact excitation of B-like Fe XXII. A detailed comparison of the *R*-matrix and RDW results is carried out. In contrast to the previous close-coupling studies of this ion, we do not detect significant discrepancies between the two methods for the background collision strengths of most transitions, including some strong excitations where large differences have been reported. We also show that at energies above ~1.5 keV, the partial waves with $l>40$ contribute significantly to the strong dipole transitions, and the Coulomb-Bethe approximation is an accurate method to account for such contributions. The isolated-resonance approximation is shown to give reasonable accuracy of 10–20 % for the resonance contributions to the effective collision strengths. The radiation damping effect as indicated by the isolated-resonance approximation appears to be far less important than those obtained with the previous Breit-Pauli *R*-matrix method. We suggest a close examination and comparison of the existing *R*-matrix implementations in order to resolve these discrepancies.

ACKNOWLEDGMENT

This work is supported by NASA Grant No. NAG5-5419.

[1] H. L. Zhang and D. H. Sampson, At. Data Nucl. Data Tables **56**, 41 (1994).
[2] H. L. Zhang and A. K. Pradhan, Phys. Rev. A **50**, 3105 (1994).
[3] H. L. Zhang and A. K. Pradhan, J. Phys. B **28**, L285 (1995).
[4] H. L. Zhang and A. K. Pradhan, Astron. Astrophys., Suppl. Ser. **123**, 575 (1997).
[5] S. Ait-Tahar, I. P. Grant, and P. H. Norrington, Phys. Rev. A **54**, 3984 (1996).
[6] M. F. Gu, Astrophys. J. **582**, 1241 (2003).
[7] J. J. Chang, J. Phys. B **10**, 3335 (1975).
[8] P. H. Norrington and I. P. Grant, J. Phys. B **20**, 4869 (1987).
[9] P. G. Burke, A. Hibbert, and W. D. Robb, J. Phys. B **4**, 153 (1971).
[10] P. J. A. Buttle, Phys. Rev. **160**, 719 (1967).
[11] I. G. Young and P. H. Norrington, Comput. Phys. Commun. **83**, 215 (1994).
[12] K. L. Baluja, P. G. Burke, and L. A. Morgan, Comput. Phys. Commun. **27**, 299 (1982).
[13] H. L. Zhang, D. H. Sampson, and A. K. Mohanty, Phys. Rev. A **40**, 616 (1989).
[14] A. Burgess and V. B. Sheorey, J. Phys. B **7**, 2403 (1974).